PURPOSE-LED
PUBLISHING™

PAPER

Observation of superconductivity in the intermetallic compound β-IrSn$_4$

View the article online for updates and enhancements.

Observation of superconductivity in the intermetallic compound β-IrSn$_4$

Vinh Hung Tran, Zbigniew Bukowski, Piotr Wiśniewski, Lan Maria Tran and Andrzej J Zaleski

Institute of Low Temperature and Structure Research, Polish Academy of Sciences, PO Box 1410, 50-950 Wrocław, Poland

E-mail: V.H.Tran@int.pan.wroc.pl

Abstract
Low-temperature dc-magnetization, ac electrical resistivity and specific heat measurements were performed on single crystals of the intermetallic compound β-IrSn$_4$. The compound crystallizes in the tetragonal MoSn$_4$-type structure (space group $I4_1/acd$) and exhibits superconductivity below $T_c = 0.9 \pm 0.05$ K. Further, the magnitude of the ratios $\Delta C_p/(\gamma_n k_B T_c) = 1.29$, $2\Delta/(k_B T_c) = 3.55$ and of the electron–phonon coupling $\overline{\lambda}_{e-ph} = 0.5$ imply that superconductivity in β-IrSn$_4$ can be ascribed to a s-wave weak coupling regime. We determined crucial thermodynamic characteristics of the superconducting state. It turned out that depending on the assumption of either a spherical or non-spherical Fermi surface, the superconductivity can be ascribed to either a type-I and type-II/1 or type-II in clean limit, respectively. However, the behavior of the upper critical field and the anisotropic crystalline structure of the studied compound provide strong support to the type-II superconductivity. In the normal state the resistivity exhibits a prominent quadratic temperature dependence, which together with a large Kadowaki–Woods ratio and with the enhanced effective mass indicate that the electrons in β-IrSn$_4$ are strongly correlated.

(Some figures may appear in colour only in the online journal)

1. Introduction

Among various subjects of condensed matter physics, superconductivity has been attracting much attention. Interest at present mainly concerns the search for superconductors with high critical temperatures or establishing the proper mechanisms of Cooper pairing in so-called unconventional superconductors. The theme of the type-I BCS superconductivity is generally considered to be less interesting. This is owing to the fact that the type-I superconductivity occurs mostly in simple elemental metals or metalloids and the mechanism underlying the superconductivity is basically the well-known electron–phonon interaction. Curiously, type-I superconductivity has recently been found in several binary and ternary compounds, for instance, YbSb$_2$ [1, 2], TaSi$_2$ [3], (Sc, Lu)Ga$_3$ [4], LaPd$_2$Ge$_2$ [5], LaRh$_2$Si$_2$ [6], (Lu, Y, La)Pd$_2$Si$_2$ [6] and LaRhSi$_3$ [7]. These discoveries have not only broken the exclusive association between type-I superconductivity and elemental metals, but have

encouraged further investigation of type-I superconductivity, since a field-dependent anisotropic order parameter in the superconducting state has been considered for LaRhSi$_3$ [7].

Intermetallic IrSn$_4$ binary crystallizes in three modifications; the low-temperature form, so-called α-IrSn$_4$, adopts the trigonal IrGe$_4$-type structure (space group $P3_121$) [8], the high-temperature form, β-IrSn$_4$ has the tetragonal MoSn$_4$-type structure (space group $I4_1/acd$) [9], and the high-pressure form, HP-IrSn$_4$, possesses the orthorhombic PtSn$_4$-type structure (space group $Ccca$) [10, 11]. The structures of the two latter modifications stand in close relation to each other. To the best of our knowledge, only α-IrSn$_4$ was reported to be a Pauli paramagnet and non-superconducting down to 2 K [8], whereas none of physical properties of β-IrSn$_4$ and HP-IrSn$_4$ have been reported yet.

In this work, we present magnetization, electrical resistivity and specific heat measurements on single crystals of intermetallic compound β-IrSn$_4$, which becomes supercon-
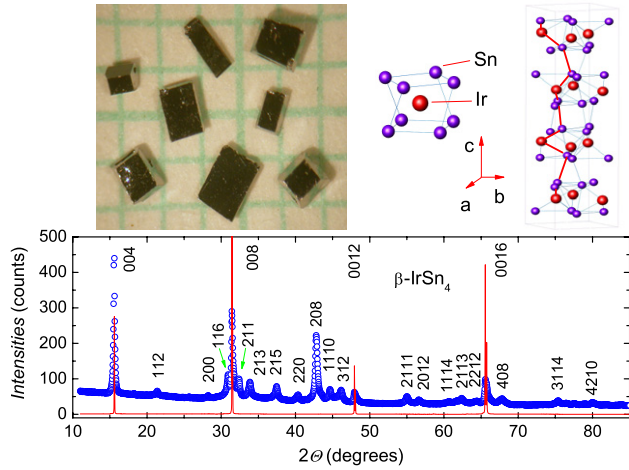
Figure 1. Left upper panel shows a photograph of grown single crystals. Right upper graph shows the square antiprism formed by eight Sn atoms with the central Ir atom and the schematic crystal structure of β-IrSn$_4$. The thick line joining atoms indicates the shortest interatomic distances. The bottom panel is the powder x-ray diffraction pattern (small circle symbols) compared to a single crystal diffraction pattern (solid line) obtained using an x-ray beam perpendicular to the 00l plane.

ducting with a transition temperature T_c of 0.9 ± 0.05 K. Although the zero-field data characterize β-IrSn$_4$ well as a s-wave weakly coupled type-I superconductor in a dirty limit, from an estimation of some thermodynamic parameters we arrive at a conclusion that superconductivity in β-IrSn$_4$ can be ascribed to a type-II superconductor in a clean limit with an assumption of a non-spherical Fermi surface.

2. Single crystal growth and crystallographic characterization

Single crystals of β-IrSn$_4$ were grown by the self-flux method. A mixture of high-quality elemental metals Ir (purity 99.99%) and Sn (at. 99.999%) with the atomic ratio Ir:Sn = 1:80 was placed in an alumina crucible, sealed in an evacuated quartz ampule, and heated up to 900 °C. After cooling down to 600 °C at a rate of 5 °C h^{-1}, the furnace was turned off and the quartz ampule was slowly cooled down to 300 °C within 3 h. Then, liquid Sn flux was decanted and the excess of Sn was removed by etching in HCl. Single crystals were obtained in the form of regular geometric shapes (see the left upper panel of figure 1).

X-ray powder diffraction of powdered small crystals and single crystal diffraction of a crystal were performed at room temperature using a X'Pert PRO x-ray diffractometer with monochromatized Cu Kα radiation. Since powdered small crystals possess texture, lattice parameters were calculated from the positions of the Bragg peaks only. Two alternative models of the crystal structure were considered, i.e., the tetragonal MoSn$_4$-type structure and the orthorhombic PtSn$_4$-type structure. Our analysis indicated that all the observed Bragg lines on the x-ray diffraction patterns could be indexed on the basis of the tetragonal MoSn$_4$-type structure with the lattice parameters $a = 0.6308(2)$ nm and $c =$

2.2739(4) nm (see the bottom panel of figure 1). The lattice parameters of our sample are in good agreement with those previously reported ($a = 0.6309$ nm and $c = 2.2770$ nm) [9]. The single crystal diffraction pattern (solid line) shows only 00l reflections, indicating that the crystallographic c-axis is perpendicular to the widest surface of the crystals.

Taking into account the atomic positions of Ir(8b) and Sn(32g) [9], we show the crystal structure of β-IrSn$_4$4 in the right upper panel of figure 1. In this tetragonal MoSn$_4$-type structure, the Ir atoms are coordinated by eight Sn atoms. The eight Sn atoms form a square antiprism, which together with other antiprisms establish infinite layers. Further, the structure can be described as a stacking of four layers of IrSn$_8$ antiprisms. The atoms are arranged in the sequence, 4Sn–Ir–4Sn...4Sn–Ir–4Sn...4Sn–Ir–4Sn...4Sn–Ir–4Sn along the c-direction. The minimum interatomic distances within layers are $d_{Sn-Sn} = 0.309$ and $d_{Ir-Ir} = 0.446$ nm. Because of a large d_{Ir-Ir}, the direct Ir–Ir interactions are almost excluded. Thus, the closer Sn–Sn contacts are favorable for an in-plane charge-carrier flow within the Sn layers. However, we recognize that interatomic distances $d_{Ir-Sn} = 0.275$ nm and $d_{Sn-Sn} = 0.296$ nm between layers are even shorter than these within the plane. This means that dominant charge carriers would take a path ...Ir–Sn–Sn–Ir–Sn–Sn–Ir... along the shortest interatomic distances, i.e., the chain along the c-axis. In considering the origins of the physical behavior discussed below, the fact that the Ir and Sn atoms in the unit cell are nearest neighbors may suggest overlap of the Sn sp-orbitals with Ir d-orbitals as mostly responsible for the electron transport properties in β-IrSn$_4$.

3. Physical properties

Dc-magnetization measurement was carried out using a commercial SQUID magnetometer (Quantum Design MPMS-XL) with an iQuantum ^{3}He outfit. For the measurement, several single crystals were glued together to get a specimen of 18 mg. In figure 2(a) we present the temperature dependence of the magnetization $M(T)$ collected at several magnetic fields. The data at 1.5 mT reveal a large diamagnetic signal below $T_c(1.5$ mT$) = 0.95$ K, indicating a superconducting transition. It is interesting to note that the onset of the superconductivity in 2 mT occurs at the same T_c as in 1.5 mT. With further increasing fields, T_c shifts down to lower temperatures, the diamagnetic signal at 0.45 K becomes stronger and simultaneously the transition becomes sharper. The latter finding may suggest that superconductivity becomes more homogeneous with magnetic fields. Figure 2(b) shows the isothermal magnetization measured at a temperature around 0.5 K. The hysteresis of the magnetization in the superconducting state resembles the behavior of both type-I and type-II superconductors with comparable coherence lengths and penetration depths. If β-IrSn$_4$ is a type-I superconductor then the departure from the discontinuous jump transition at the critical field can be ascribed to a strong pinning of domain walls in the intermediate state or to an unaccounted demagnetization factor. In this case, the thermodynamic
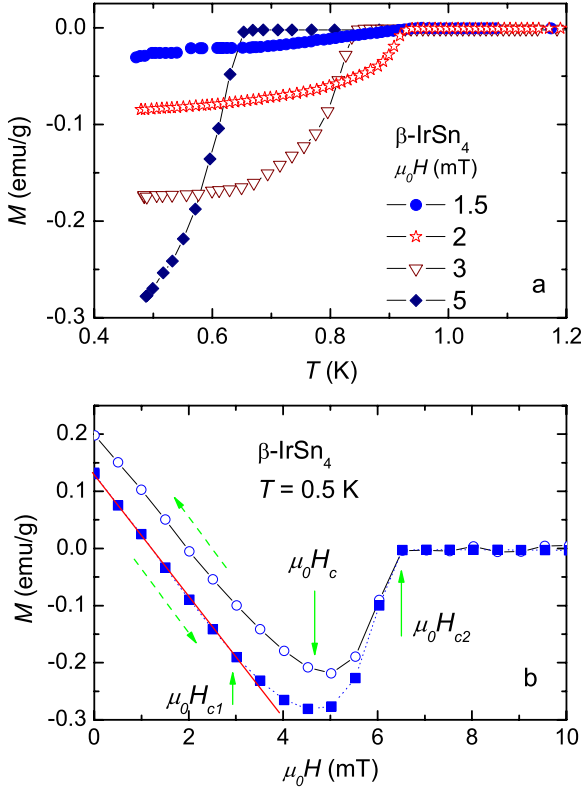
Figure 2. (a) Zero-field cooled dc-magnetization at several magnetic fields as a function of temperature. (b) Isotherms measured at 0.5 K. The dashed arrows indicate the sweeping direction of the applied magnetic fields. The solid arrows denote the critical fields $\mu_0 H_{c1}$, $\mu_0 H_c$ and $\mu_0 H_{c2}$.

Figure 3. (a) Field-dependent electrical resistivity of β-IrSn$_4$ around the superconducting phase transition. The dotted line indicates the middle point of the transition. (b) Field dependence of the resistivity at 0.45 K. The arrow denotes the midpoint of the transition and is taken as an upper critical field.

critical field $\mu_0 H_c$ can be estimated to be approximately 4.7 mT. If β-IrSn$_4$ is considered as a type-II superconductor then one can estimate the lower critical field $\mu_0 H_{c1}$ and the upper critical field $\mu_0 H_{c2}$. $\mu_0 H_{c1} = 3$ mT, if is defined as the field where the deviation of the $M(H)$ curve from linearity in the Meissner state sets in, while $\mu_0 H_{c2} = 6.5$ mT at 0.5 K, determined as the intersection between linear interpolations of the magnetization in the superconducting and normal states. The positions of the critical fields are denoted by solid arrows in figure 2(b). Above $\mu_0 H_{c2} = 6.5$ mT or in the normal state the studied compound behaves like a Pauli paramagnet.

Electrical resistivity was measured using a conventional four-probe ac-technique with an in-plane current of 0.5 mA and frequency of 37 Hz. The gold wires for electrical contracts were attached to samples using silver paste. The two measured samples have dimensions of $0.36 \times 1.68 \times 0.18$ mm^3, $1.2 \times 0.74 \times 0.1$ mm^3, respectively. The measurements were carried out using a Quantum Design physical property measurement system (PPMS) with a ^{3}He cooler. Several selected magnetic fields up to 10 mT were applied parallel to the c-axis. The experimental data obtained on the two samples were reproducible. The typical value of the remnant field is less than 0.5 mT when decreasing the field from 10 mT in the oscillating mode. For measurements in fields below 2 mT, the bias field was further removed to get a lower remnant field, below 0.2 mT, before cooling the sample from room temperature. The strength of the remnant fields was controlled
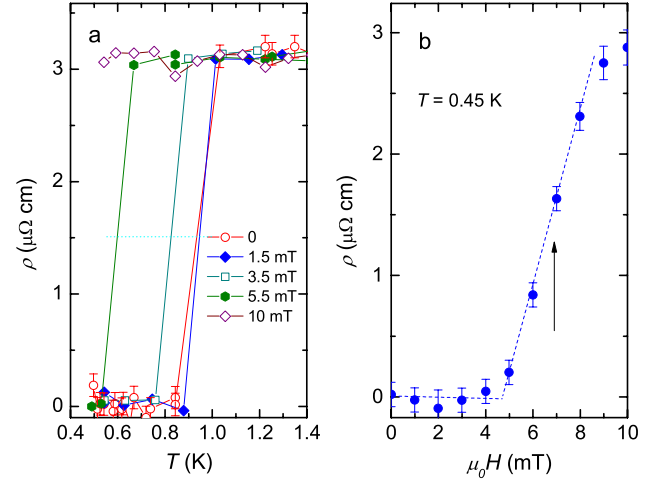
by an Applied Physics Systems Fluxgate Model 150–6325 magnetometer.

Low-temperature data shown in the upper inset of figure 3(a) indicate that the resistivity starts to drop abruptly at 1 K and arrives at zero value at 0.84 K. The critical temperature, T_c, defined as a middle point of the superconducting transition, and the transition width, $\Delta T_c = T_c(90\%) - T_c(10\%)$, are determined to be 0.93 K and 0.15 K, respectively. Upon increasing the magnetic fields, the superconducting transition shifts to lower temperatures and even a small field of 10 mT is sufficient to reduce the T_c to less than 0.5 K. From the field dependence of the resistivity we have determined the upper critical field. At 0.45 K $\mu_0 H_{c2} = 6.8$ mT (see figure 3(b)), which is in good agreement with the value obtained from the magnetization measurements.

In figure 4 we show the electrical resistivity of β-IrSn$_4$ in the temperature range 0.35–300 K. The temperature dependence of $\rho(T)$ indicates that this intermetallic is a good metal. At room temperature the resistivity amounts to 80 $\mu\Omega$ cm and decreases to approximately 3 $\mu\Omega$ cm at 1 K. A large residual resistivity ratio RRR = 27, sharp superconducting transition and small residual resistivity value manifest the good sample quality and negligible scattering by defects and impurities. The resistivity just above T_c follows a quadratic temperature dependence $\rho(T) = \rho_0 + AT^2$, as shown in the inset of figure 4 by the solid line. By fitting this formula to the data between 1 and 15 K we obtained the residual resistivity of $\rho_0 = 3.2$ $\mu\Omega$ cm and the coefficient $A = 0.9 \times 10^{-3}$ $\mu\Omega$ cm K^{-2}. It is apparent that the A-coefficient is greatly enhanced, as compared to those observed for transition metals with A of the order of magnitude of 10^{-5} $\mu\Omega$ cm K^{-2} [12]. The observation of the $\rho \propto T^2$ dependence and a relatively large A coefficient are symptomatic of strong electron–electron interactions in the Fermi-liquid state of β-IrSn$_4$. At higher temperatures, a curvature of the resistivity suggests to analyze it in terms of
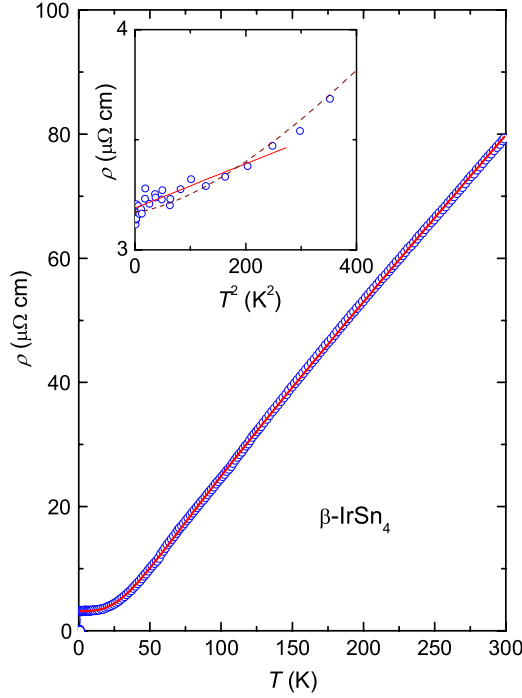
Figure 4. Temperature dependence of the resistivity of β-IrSn$_4$ (circle symbols) with a Bloch–Grüneisen–Mott fit (solid line). The inset shows the resistivity versus T^2 with a solid line representing the T^2 fit and dashed line denoting the Bloch–Grüneisen–Mott fit.

the Bloch–Grüneisen relation [13]. We fitted the experimental data to equation (1) and found that the residual resistivity $\rho_0 = 3.17$ $\mu\Omega$ cm, the coefficient $k = 112$ $\mu\Omega$ cm, the Debye temperature $\Theta_D = 216$ K and the exponent $n = 3$. The observed value $n = 3$ and a good agreement between theory and the experimental data up to room temperature implies a significant s–d band scattering.

$$\rho(T) = \rho_0 + k \left(\frac{T}{\Theta_D}\right)^n \int_0^{\Theta_D/T} \frac{x^n dx}{(e^x - 1)(1 - e^{-x})}. \quad (1)$$

The Hall effect was measured on one of the samples used in the resistivity measurements. We utilized a Quantum Design Horizontal Rotator in a Quantum Design PPMS platform to rotate the sample from 0° to 180°. The Hall resistivity data, determined as $\rho_H = \frac{1}{2}(\rho_{H,0°} - \rho_{H,180°})$, were collected at 2 K and in fields up to 9 T using a conventional four-probe ac-technique with an in-plane current of 0.5 mA and frequency of 37 Hz. Figure 5 depicts the experimental Hall resistivity. The data show that ρ_H is linearly proportional to $\mu_0 H$ up to 2 T. At high fields, ρ_H deviates from the initial linear dependence. The reason for the nonlinear $\rho_H(H)$ behavior is not ascertained as yet. One suspects that it may arise from a new contribution associated with spin–orbit coupling, which is negligible in a low-field regime but becomes perceptible in high fields. Alternatively, one can consider the observed field dependence of the Hall resistivity as due to competing contributions of two carrier types with different densities and mobilities. In the low-field limit, the Hall coefficient is dominated by the ordinary term R_0 and can
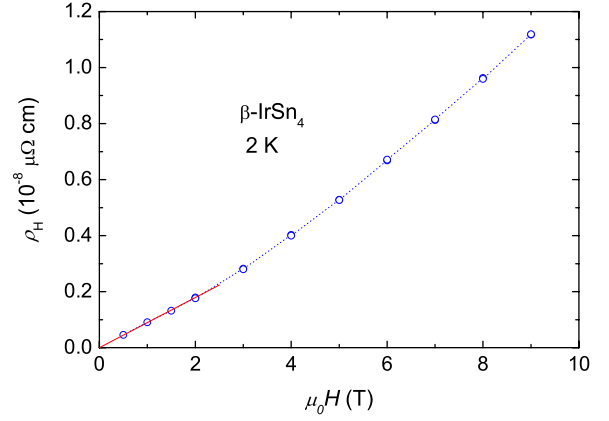

Figure 5. Field dependence of the Hall resistivity of β-IrSn$_4$ at 2 K. Solid line represents a linear fit of the Hall resistivity in the low-field regime.

be estimated by $R_0 = \rho_H/(\mu_0 H) = 8.95 \times 10^{-10}$ m^3 C^{-1}. In the simple one-band approximation, the ratio $1/(R_0 e)$, where e is the elementary charge, may be interpreted as an effective charge-carrier concentration. We estimated the number of carriers, $n = 1/(R_0 e) = 6.98 \times 10^{27}$ m^{-3}. Because the Hall coefficient is positive at all fields measured, it implies that the charge carriers are predominantly hole-like. The Hall ordinary term R_0 can be combined with the resistivity data to obtain the Hall mobility μ_H and Hall mean free path l_H. From the equations $\mu_H = R_0/\rho$ and $l_H = \hbar^2(3\pi^3/e^4)^{1/3}R_0^{2/3}/\rho$ we estimated $\mu_H = 280$ cm^2 V^{-1} s^{-1} and $l_H = 109$ nm, respectively.

The specific heat was measured by the thermal relaxation method on a sample of ~1 mg. The specific heat measurements were done using the same setup and experimental conditions as the electrical resistivity. We carried out careful calibration of the calorimeter and measurement of addenda before the proper measurements were done. The zero-field specific heat of β-IrSn$_4$ divided by temperature, C_p/T, versus T^2 is depicted in figure 6(a). The normal state specific heat follows the standard law for metals $C_p = \gamma_n T + \beta T^3$, where γ_n and β are the normal state electronic heat and phonon specific heat coefficients, respectively. A linear fit of the data to $C_p/T = \gamma_n + \beta T^2$ yields $\gamma_n = 5.2 \pm 0.2$ mJ mol^{-1} K^{-2} and $\beta = 0.91 \pm 0.15$ mJ mol^{-1} K^{-4}. Knowing the β value, we can determine the Debye temperature: $\Theta_D = (12\pi^4 rR/5\beta)^{1/3} = 221 \pm 8$ K, in a good agreement with the value Θ_D deduced from the resistivity data (where $r = 5$ is the number of atoms per formula unit and R is the gas constant). In order to get some information on the strength of the electron–phonon coupling we estimate the average electron–phonon coupling constant $\bar{\lambda}_{e–ph}$ using the McMillan equation [14]:

$$\bar{\lambda}_{e–ph} = \frac{1.04 + \mu^* \ln(\Theta_D/1.45T_c)}{(1 - 0.62\mu^*) \ln(\Theta_D/1.45T_c) - 1.04} \quad (2)$$

where μ^* is the Coulomb pseudopotential, usually assumed to be between 0.1 and 0.15 [14, 15]. For $\mu^* = 0.15$, $\Theta_D = 221$ K and $T_c \approx 0.9$ K, equation (2) yields $\bar{\lambda}_{e–ph} = 0.5$, suggestive of a weak electron–phonon coupling in β-IrSn$_4$.

Figure 7. The specific heat divided by temperature $C_p(T)/T$ in various magnetic fields plotted versus temperature squared.

of $\Delta C_p/T_c$ means that the transition order changes from the second order in zero-field to the first order in applied magnetic fields. A similar behavior has been observed in the type-I superconductors (Sc, Lu)Ga$_3$ [4] and LaRhSi$_3$ [7], thus strongly supporting a type-I superconductivity in β-IrSn$_4$. Second, perhaps most surprisingly, the critical temperature increases a little, up to 0.94 K, on the application of a field of 1.5 mT. The same T_c value was obtained from the C_p-data at 2 mT. Because the used field strength is much larger than the remnant field ($<$0.5 mT), the measurement artifact can be excluded. Moreover, the values of the critical temperature T_c are reproduced in independent measurements of specific heat and magnetization on different samples. Therefore, it is most likely that the slight enhancement of T_c upon application of the magnetic fields is an intrinsic property of the studied samples.

In figure 8(a) we show the effect of applied magnetic fields on the Sommerfeld ratio $C_p(H)/T$ at 0.4 K. Apparently, $C_p(H)/T$ is not linear in field. Similarly to the case of LaRhSi$_3$ [7] one describes the field dependence of the $C_p(H)/T$ data by the exponential function $C_p(H)/T = \gamma(0.4\ \text{K}) + A \times \exp(-H^*/H)$, where $\gamma(0.4\ \text{K})$, A and $\mu_0 H^*$ are fitting parameters. The best fit for data collected in magnetic fields below 7 mT gives $\gamma(0.4\ \text{K}) = 3.9$ mJ mol^{-1} K^{-2}, $A = 15.8$ mJ mol^{-1} K^{-2} and $\mu_0 H^* = 9.5$ mT. The exponential field dependence of $C_p(H)/T$ in the tetragonal superconducting LaRhSi$_3$ has been attributed to a change in the superconducting gap, which is isotropic in zero-field but becomes anisotropic in applied magnetic fields [7]. Since a similar nonlinearity of $C_p(H)/T$ is observed in LaRhSi$_3$ and β-IrSn$_4$, one may think that the effect reported for β-IrSn$_4$ can be explained in the same frame as has been used for LaRhSi$_3$. However, because our specific heat data were collected on single crystals, i.e. for $\mu_0 H \parallel c$-axis, our data should reflect the field dependence of the superconducting gap along one direction only, thus contradict the anisotropic model of the superconducting gap. To unravel the strong field dependence of $C_p(H)/T$ in β-IrSn$_4$, we propose to consider $C_p(H)/T$ in two field ranges: below 2.5 mT, where $C_p(H)/T$ is independent of magnetic fields,
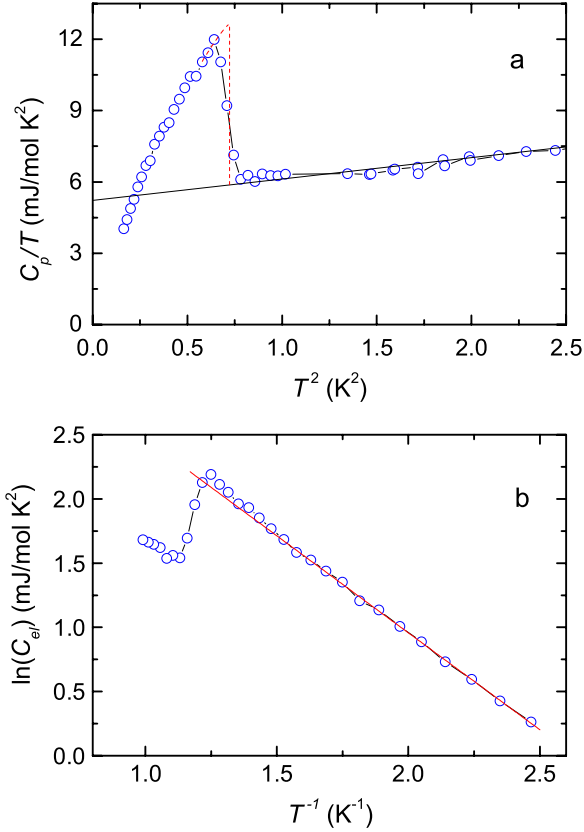
Figure 6. (a) Specific heat of β-IrSn$_4$ divided by temperature C_p/T as a function of temperature squared in zero magnetic field. The solid line indicates the linear behavior in $C_p/T = \gamma_n + \beta T^2$. The dashed line is a guide for the eye. (b) The electronic specific heat on a logarithmic scale as a function of $1/T$. The solid line presents the exponential function given by the BCS theory $C_{el}(T) = A\gamma_n T_c \exp(-\Delta_0/k_B T)$, with $A = 12.8$ and $\Delta_0/k_B = 1.51$ K.

The bulk nature of superconductivity in β-IrSn$_4$ is evidenced by a clear peak in the $C_p(T)/T$ dependence. The critical temperature $T_c = 0.85$ K, taken as the middle point of the $\Delta C_p(T)/T$ jump, agrees fairly with that deduced from the resistivity. We determined the ratio $\Delta C_p/\gamma_n T_c = 1.29$, which is noticeably smaller than 1.43 given by the BCS theory for weakly coupled superconductors. In figure 6(b) we show the $\ln(C_{el}(T))$ versus $1/T$ dependence, where $C_{el}(T) = \Delta C_p(T) = C_p(T) - \beta T^3$ is the electronic specific heat. It is clear that in the superconducting state $C_{el}(T)$ follows a single-gapped BCS-like function $C_{el}(T) = A\gamma_n T_c \exp(-\Delta_0/k_B T)$. For the temperature range 0.4–0.7 K we obtained an energy gap $\Delta_0/k_B = 1.51$ K, corresponding to $2\Delta_0/k_B T_c = 3.55$ and parameter $A = 12.8$. The two latter values are comparable to those of weak coupling BCS superconductors: 3.52 and 8.5, respectively. This and the value of the ratio $\Delta C_p/\gamma_n T_c$ consistently imply that β-IrSn$_4$ is a weak coupled superconductor.

The plot of $C_p(T)/T$ measured in various magnetic fields up to 7 mT is shown in figure 7. The main points to note from this figure are the following: first, the specific heat jump $\Delta C_p/T_c$ in small magnetic fields, namely in 1, 1.5 and 2 mT, is larger than that in zero-field. The observed field dependence
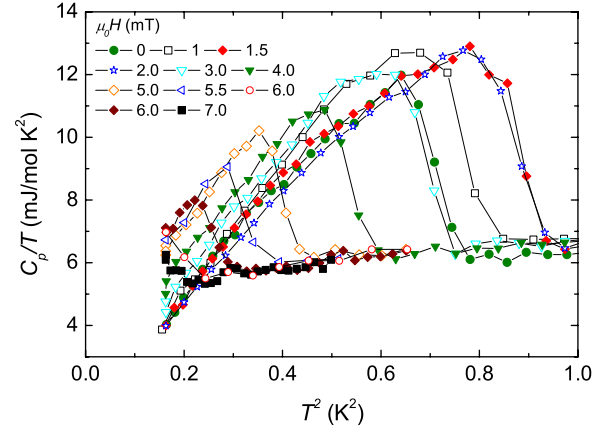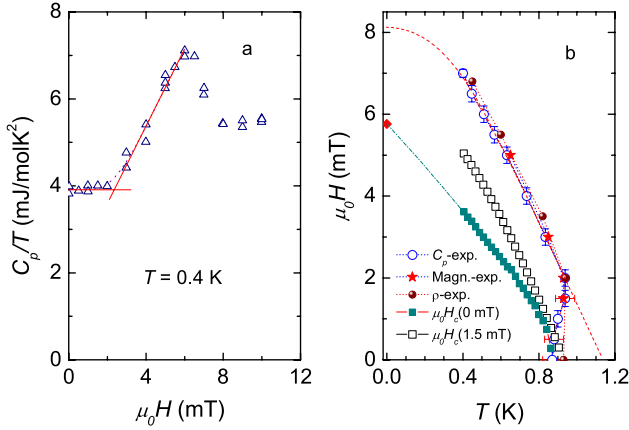
Figure 8. (a) Field dependence of the Sommerfeld ratio $C_p(H)/T$ at 0.4 K. The dotted line is a fit to $\exp(-H^*/H)$ with $\mu_0 H^* = 9.5$ mT. The solid lines express the behavior of $C_p(H)/T$ in two magnetic field regimes: below $\mu_0 H_{c1}$, and between $\mu_0 H_{c1}$ and $\mu_0 H_{c2}$. (b) Temperature dependence of the critical field $H_c(T)$ determined from measurements of the specific heat (open circles), magnetization (closed stars) and electrical resistivity (bullets) under applied magnetic fields and that calculated from free-energy considerations of specific heat data at zero-field (closed squares) and 1.5 mT (open squares). The dashed line represents the theoretical WHH model with $T_{c0} = 1.14$ K and $\mu_0 dH_{c2}/dT = -9.83$ mT K^{-1} while the dashed–dotted line is a guide to the eye.

and in the field range 2.5–6 mT, where $C_p(H)/T$ follows magnetic fields linearly. These two field regimes correspond approximately to those below $\mu_0 H_{c1}$, and between $\mu_0 H_{c1}$ and $\mu_0 H_{c2}$, respectively. We note that for a standard BCS superconductor with a single isotropic energy gap, $C_p(H)/T$ should increase linearly in magnetic fields, until the flux lines start to overlap. Such a linear field dependence of $C_p(H)/T$ is found for applied fields larger than the lower critical field, when the non-superconducting density of states develops with an increasing number of flux lines. Obviously, in fields smaller than $\mu_0 H_{c1} \sim 3$ mT, $C_p(H)/T$ should be practically independent of fields since the magnetic flux penetrating into the material is only in a very thin layer of the surface and the contribution of the non-superconducting density of states to the total density at the Fermi level is negligible.

From our measurements of magnetization, electrical resistivity and specific heat we deduced the critical fields $\mu_0 H_{c2}(T)$. The resulting H–T phase diagram is shown in figure 8(b). In this figure we compare also the temperature dependences of the thermodynamic critical fields $\mu_0 H_c(T)$ calculated from the C_p-data at 0 and 1.5 mT. The theoretical $\mu_0 H_c(T)$ values have been obtained by integrating the difference of specific heats between the superconducting (s) and normal (n) state and integrating the difference of the specific heats divided by temperature according to the formulas:

$$-\tfrac{1}{2}\mu_0 V_M H_c^2(T) = \Delta F(T) = \Delta U(T) - T\Delta S(T) \quad (3a)$$

$$\Delta U(T) = \int_T^{T_c} [C_s(T') - C_n(T')] \mathrm{d}(T') \quad (3b)$$

$$\Delta S(T) = \int_T^{T_c} \frac{[C_s(T') - C_n(T')]}{T'} \mathrm{d}(T'), \quad (3c)$$

where $\Delta U(T)$ is the internal energy difference and $\Delta S(T)$ is the entropy difference. Using the relation $\mu_0 V H_c^2(0) = (3\gamma_n/2\pi^2 k_B^2)(\Delta_0/k_B)^2$, the values $\gamma_n = 5.2 \times 10^{-3}$ J mol^{-1} K^{-2}, $V_M = 68.24 \times 10^{-6}$ m^3 mol^{-1} and $\Delta_0 = 1.51$ K we obtained $\mu_0 H_c(0) = 5.76$ mT at 0 K. This value is denoted by a solid diamond in figure 8(b). Clearly, there is an essential deviation of the experimental $\mu_0 H_{c2}(T)$ data from the thermodynamic field deduced from the entropy balance. This behavior indicates that β-IrSn$_4$ should be a type-II superconductor in magnetic fields. A comparison of the calculated thermodynamic critical fields at 0 and 1.5 mT indicates that the temperature dependence of $\mu_0 H_c(T)$ is sensitive to applied magnetic fields.

A remarkable finding of our measurements is that $T_c(H_{c2}) = 0.85$ K at zero field attains its maximum value of 0.94 K in fields 1.5 and 2 mT. This behavior resembles the situation found for Eu$_x$Sn$_{1-x}$Mo$_6$S$_8$ [16], λ-(BETS)$_2$FeCl$_4$ [17], URhGe [18] and Eu(Fe$_{0.81}$Co$_{0.18}$)$_2$As$_2$ [19], namely superconductivity can be induced or the critical temperature can be increased by the application of suitable magnetic fields. The analogy between β-IrSn$_4$ and the mentioned superconductors is not obvious because the observed effect in β-IrSn$_4$ occurs just below $\mu_0 H_{c1}$ and is rather obscure. Therefore, further investigations will be required in order to establish the proper mechanism of the unusual $T_c(H)$ dependence observed in β-IrSn$_4$.

Another aspect worth considering is the almost linear behavior of $H_{c2}(T_c)$ above 2 mT. In fact, a fit of the conventional relation $H_{c2}(T) = H_{c2}(0)[1 - (T/T_c(0))^n]$ to the experimental data gives the critical field $H_{c2}(0) = 9.55$ mT, critical temperature $T_c(0) = 1.13$ K and exponent $n = 1.25$. The latter value is significantly reduced in respect to $n = 2$ expected from the BCS theory.

We calculated the upper critical field using the model developed by Werthamer *et al* [20] (WHH model) for a type-II superconductor. Taking the slope of $\mu_0 H_{c2}(T)$ in the temperature range 0.63–0.94 K, $\mathrm{d}\mu_0 H_{c2}(T)/\mathrm{d}T = -9.83$ mT K^{-1}, and the orbital-limiting field relation $\mu_0 H_{c2}^{orb} = 0.73 T_c(0)[-\mathrm{d}\mu_0 H_{c2}(T)/\mathrm{d}T]_{T_c}$ for a clean limit superconductor, we obtain $\mu_0 H_{c2}^{orb} = 8.1$ mT for $T_c(0) = 1.13$ K. It appears that all observed values of the critical fields are small and certainly indicate the absence of the Pauli limiting field $\mu_0 H_p = 1.86 T_c$, which is of the order of $\sim$2 T. In order to support the dominant orbital-pair breaking effect we determined the value of the Maki parameter [20, 21], $\alpha_M = (3e^2\hbar\gamma_V\rho_0)/(2\pi^2 k_B^2 m_e) = 5.4 \times 10^{-3}$. In the formula, $\gamma_V = 76.2$ J m^{-3} K^{-2} is the electronic specific heat coefficient per volume and m_e is the electron mass. On the other hand, from the relation $\alpha_M = 0.528 \times [-\mathrm{d}H_{c2}(T)/\mathrm{d}T]_{T_c}$ [20, 21], with $\mathrm{d}H_{c2}(T)/\mathrm{d}T$ in the units of T K^{-1}, the value of the Maki parameter is $\approx 5.2 \times 10^{-3}$, i.e., very close to the above value.

It is of considerable interest to estimate some thermodynamic parameters characterizing the superconducting state. First, we calculated the Fermi wavenumber $k_F = (3\pi^2 n_s)^{1/3} = 4.65 \times 10^9$ m^{-1}, where the superconducting carrier density $n_s = 3.39 \times 10^{27}$ m^{-3} is a half of the total electron density n and e is the elementary charge. Then, we determined the effective mass $m^* = 3\hbar^2\gamma_V/(k_B^2 k_F) \sim$

3.1 m_e. The London penetration depth $\lambda_{\rm L}(0) = 162$ nm can be obtained from the formula: $\lambda_{\rm L}(0) = \sqrt{\frac{m^* c^2}{4\pi n_s e^2}}$, where c is the speed of light. On the other hand, using the BCS relation for the coherence length $\xi_0 = 0.18\hbar\upsilon_{\rm F}/k_{\rm B}T_{\rm c}$, we obtained $\xi_0 = 261$ nm, where $\upsilon_{\rm F} = \hbar k_{\rm F}/m^* = 1.71 \times 10^5$ m s^{-1} is the Fermi velocity. The obtained ratio $\kappa(0) = \lambda_{\rm L}(0)/\xi_0 \approx 0.62 < 1/\sqrt{2}$ suggests ascribing the superconductivity in β-IrSn$_4$ to either a type-I or to a type-II/1 in the classification of Auer and Ullmaier [22]. Further, using the formulas given by Orlando *et al* [23], we can estimate the BCS coherence length $\xi_0 = 7.95 \times 10^{-17} n_s^{2/3} S/S_{\rm F}/[\gamma_V T_{\rm c}]$ and London penetration depth $\lambda_{\rm L}(0) = 1.33 \times 10^8 \gamma_V^{1/2}/[n_s^{2/3} S/S_{\rm F}]$. In this estimation, uncertainties may appear due to the unknown ratio of the Fermi surface of the superconducting electrons, S, to the surface of the free electrons $S_{\rm F}$, $S/S_{\rm F}$. Therefore, we will consider two extreme cases, namely assuming a spherical Fermi surface ($S/S_{\rm F} = 1$) or non-spherical Fermi surface (e.g. $S/S_{\rm F} = 0.35$). The first assumption yields $\xi_0 = 262$ nm, $\lambda_{\rm L} = 163$ nm, whereas with the latter one we obtain $\xi_0 = 92$ nm, $\lambda_{\rm L} = 465$ nm. Correspondingly, the electronic mean free path $l_e = 1.27 \times 10^4/[\rho_0 n_s^{2/3}(S/S_{\rm F})]$ amounts to 521 or 1489 nm, respectively. Because l_e is always larger than ξ_0, the superconductivity in β-IrSn$_4$ is certainly in the clean limit. The estimation leads to an interesting conclusion that if the Fermi surface is spherical then $\kappa = 0.62$, so supporting type-I and type-II/1 superconductivity in β-IrSn$_4$. Conversely, if the Fermi surface is non-spherical, κ takes a value of 5, implying that the superconductivity is of type-II.

In the clean limit, the Ginzburg–Landau coherence length $\xi_{\rm GL}$ and Ginzburg–Landau parameter $\kappa_{\rm GL}$ can be estimated using the respective relations $\xi_{\rm GL} = 5.87 \times 10^{-17}/[n_s^{2/3}(S/S_{\rm F})]$ and $\kappa_{\rm GL} = 1.6 \times 10^{24} T_{\rm c}\gamma_V/[n_s^{2/3}(S/S_{\rm F})]^2$ [23]. We obtained $\xi_{\rm GL}$ and $\kappa_{\rm GL}$ values of 68 nm and 4.9, respectively, and the resulting Ginzburg–Landau penetration depth is $\lambda_{\rm GL} = \kappa_{\rm GL}\xi_{\rm GL} = 327$ nm. Also, a method of estimation of $\xi_{\rm GL}$ is based on the knowledge of the upper critical field. Assuming $\mu_0 H_{\rm c2}^{H\|c} = \mu_0 H_{\rm c2}^{\rm orb}$, an anisotropic value of the Ginzburg–Landau coherence length ξ_{ab}, which is related to $\mu_0 H_{\rm c2}^{H\|c}$ by the relation $\mu_0 H_{\rm c2}^{H\|c} = \Phi_0/(2\pi\xi_{ab}^2)$, where Φ_0 is the flux quantum. For $\mu_0 H_{\rm c}^c = 8.1$ mT this results as $\xi_{ab} = 206$ nm.

4. Discussion and conclusions

The first picture which emerges from our measurements on single crystals of β-IrSn$_4$ is that this binary intermetallic compound becomes superconducting below 0.9 ± 0.05 K. The zero-field data listed in table 1 are in accordance with the conventional s-wave singlet pairing mechanism and would also provide a hint of either the type-I or type-II/1 superconductivity with a weak electron–phonon coupling.

In order to get insight into the physics underlying the superconductivity in β-IrSn$_4$ we can discuss several factors which would be involved in the Cooper pairing mechanism: (i) anisotropy of the Fermi surface and (ii) electron correlations. First of all, on account of the fact that β-IrSn$_4$ crystallizes in the tetragonal MoSn$_4$-type structure, an anisotropy of the

Table 1. Thermodynamic parameters of the superconductor β-IrSn$_4$: critical temperature $T_{\rm c}$, critical field $\mu_0 H_{\rm c0}(0)$, electron–phonon coupling constant $\bar{\lambda}_{\rm e-ph}$, Maki parameter $\alpha_{\rm M}$, electronic heat coefficient γ_n, lattice heat coefficient β, specific heat jump $\Delta C_p/\gamma_n T_{\rm c}$, superconducting energy gap ratio $2\Delta_0/k_{\rm B}T_{\rm c}$, Fermi wavevector $k_{\rm F}$, effective masses of superconducting carriers m^*.

$T_{\rm c}$ (K)	0.9 ± 0.05
$\mu_0 H_{\rm c0}(0)$ (mT)	5.8 ± 0.1
$\alpha_{\rm M}$	5.3×10^{-3}
$\bar{\lambda}_{\rm e-ph}$	0.5 ± 0.05
γ_n (mJ mol^{-1} K^{-2})	5.2 ± 0.2
β (mJ mol^{-1} K^{-4})	0.91 ± 0.15
$\Delta C_p/\gamma_n T_{\rm c}$	1.3 ± 0.1
$2\Delta_0/k_{\rm B}T_{\rm c}$	3.55 ± 0.05
$k_{\rm F}$ ($\times 10^9$ m^{-1})	4.7 ± 0.5
m^* (m_e)	3.1 ± 0.3

Fermi surface is expected. Moreover, the assumption of a non-spherical Fermi surface leads to a deduction of the type-II superconductivity, which coincides with the observation of the upper critical field $\mu_0 H_{\rm c2}$. To examine the electron correlation factor, a determination of the Kadowaki–Wood ratio, $R_{\rm KW}$, [24, 25] is useful. Using the electronic heat coefficient $\gamma_n = 5.2$ mJ mol^{-1} K^{-2} and the T^2-resistivity coefficient $A = 0.9 \times 10^{-3}$ $\mu\Omega$ cm, the $R_{\rm KW}$ is estimated to 3.3×10^{-5} $\mu\Omega$ cm/(mJ mol^{-1} K)$^{-2}$. This value is essentially larger than the value of 1×10^{-5} $\mu\Omega$ cm/(mJ mol^{-1}K)$^{-2}$ commonly found for many correlated electron systems. Thus, we are dealing with the fact that both $R_{\rm KW}$ and the effective mass of ~ 3 m_e are enhanced in β-IrSn$_4$. This implies that the electron correlation effect, presumably due to an overlap of Sn sp-orbitals with Ir d-orbitals, would have an impact on the Cooper pairing mechanism.

Finally, an interesting outcome is obtained from comparison of the studied compound with the intermetallic compound AuSn$_4$, which was previously reported to undergo a superconducting transition at $T_{\rm c} = 2.4$ K [26, 27]. The latter compound has been shown to have an orthorhombic PdSn$_4$ structure with the noncentrosymmetric space group *Aba*2 [28]. Aside from the different crystallographic structures, the intermetallic β-IrSn$_4$ and AuSn$_4$ compounds differ in the number of d-electrons. So, the microscopic mechanisms of the electron pairing in these superconductors may be quite different.

To summarize, we have grown single crystals of intermetallic compound β-IrSn$_4$, crystallizing in the tetragonal MoSn$_4$-type structure. We have measured low-temperature magnetic, electrical resistivity and specific heat properties of the compound. We found a superconducting transition $T_{\rm c}(0{\rm T}) = 0.9 \pm 0.05$ K and an upper critical magnetic field $\mu_0 H_{\rm c2}(0) \sim 8$ mT. We have determined basic thermodynamic parameters characterizing the superconducting state, such as the specific heat jump at $T_{\rm c}$, $\Delta C_{\rm p}(T_{\rm c})/\gamma_n T_{\rm c}$, electron–phonon coupling constant, $\lambda_{\rm e-ph}$, coherence length ξ, Fermi wavevector $k_{\rm F}$, effective mass m^*, magnetic penetration depth λ, and Ginzburg–Landau parameter κ. The determined parameters are gathered in tables 1 and 2. The analysis of the experimental data allows us to characterize β-IrSn$_4$ as either a type-I as well

Table 2. Comparison of the coherence length ξ_0, London penetration depth λ_L, electron mean free path l_e, Ginzburg–Landau coherence length ξ_{GL}, Ginzburg–Landau penetration depth λ_{GL} and Ginzburg–Landau parameter κ_{GL}, estimated from the BCS theory for the spherical ($S/S_F = 1$) and non-spherical Fermi surface ($S/S_F = 0.35$).

Parameters	BCS model	$S/S_F = 1$	$S/S_F = 0.35$
ξ_0 (nm)	262 ± 5	262 ± 5	92 ± 3
λ_L (nm)	162 ± 5	163 ± 5	465 ± 10
l_e (nm)	—	521 ± 10	1489 ± 20
κ	0.62 ± 0.05	0.62 ± 0.05	5 ± 0.5
ξ_{GL} (nm)	—	193 ± 5	68 ± 2
λ_{GL} (nm)	—	115 ± 5	333 ± 10
κ_{GL}	—	0.6 ± 0.05	4.9 ± 0.5

as type-II/1 or a type-II clean limit superconductor, depending on assumption of a spherical or non-spherical Fermi surface, respectively. We favor the assumption of a non-spherical Fermi surface, since β-IrSn$_4$ crystallizes in the tetragonal MoSn$_4$-type structure. Moreover, the behavior of the upper critical field data indicates that a type-II superconductivity is realized in β-IrSn$_4$ and this interpretation does not contradict the unusual phenomena observed, including the nonlinear field dependence of the Sommerfeld coefficient and a jump in the critical magnetic field around the critical temperature, since all these anomalies may occur in the vicinity of the lower critical field $\mu_0 H_{c1}$. In the light of the observation of superconductivity on the border between the type-II and type-I in β-IrSn$_4$, the physical properties of this intermetallic compound are interesting and demand further investigation.

Acknowledgment

References

[1] Yamaguchi Y, Waki S and Mitsugi K 1987 *J. Phys. Soc. Japan* **56** 419

[2] Zhao L L, Lausberg S, Kim H, Tanatar M A, Brando M, Prozorov R and Morosan E 2012 *Phys. Rev. B* **85** 214526

[3] Gottlieb U, Lasjaunias J C, Tholence J L, Laborde O, Thomas O and Madar R 1986 *Phys. Rev. B* **45** 4803

[4] Svanidze E and Morosan E 2012 *Phys. Rev. B* **85** 174514

[5] Hull G W, Wernick J H, Geballe T H, Waszczak J V and Bernardini J E 1981 *Phys. Rev. B* **24** 6715

[6] Palstra T T M, Lu G, Menovsky A A, Nieuwenhuys G J, Kes P H and Mydosh J A 1986 *Phys. Rev. B* **34** 4566

[7] Anand V K, Hillier A D, Adroja D T, Strydom A M, Michor H, McEwen K A and Rainford B D 2011 *Phys. Rev. B* **83** 064522

[8] Lang A and Jeitschko W 1996 *J. Mater. Chem.* **6** 1897

[9] Nordmark E-L, Wallner O and Häussermann U 2002 *J. Solid State Chem.* **168** 34

[10] Larchev V I and Popova S V 1984 *J. Less-Common Met.* **98** L1

[11] Künnen B, Niepmann D and Jeitschko W 2000 *J. Alloys Compounds* **309** 1

[12] Miyake K, Matsuura T and Varma C M 1989 *Solid State Commun.* **71** 1039

[13] Ziman J M 1960 *Electrons and Phonons* (Oxford: Clarendon)

[14] McMillan W L 1968 *Phys. Rev.* **167** 331

[15] Morel P and Anderson P W 1962 *Phys. Rev.* **125** 1263

[16] Meul H W, Rossel C, Decroux M, Fischer O, Remenyi G and Briggs A 1984 *Phys. Rev. Lett.* **53** 497

[17] Uji S, Shinagawa H, Terashima T, Yakabe T, Terai Y, Tokumoto M, Kobayashi A, Tanaka H and Kobayashi H 2001 *Nature* **410** 908

[18] Levý F, Sheikin I, Grenier B and Huxley A D 2005 *Science* **309** 1343

[19] Tran V H, Zaleski T A, Bukowski Z, Tran L M and Zaleski A J 2012 *Phys. Rev. B* **85** 052502

[20] Werthamer N R, Helfand E and Hohemberg P C 1966 *Phys. Rev.* **147** 295
Helfand E and Werthamer N R 1966 *Phys. Rev.* **147** 288

[21] Maki K 1966 *Phys. Rev. B* **148** 362

[22] Auer J and Ullmaier H 1973 *Phys. Rev. B* **7** 136

[23] Orlando T P, McNiff E J Jr, Foner S and Beasley M R 1979 *Phys. Rev. B* **19** 4545

[24] Kadowaki K and Woods S B 1986 *Solid State Commun.* **58** 507

[25] Tsujii N, Yoshimura K and Kosuge K 2003 *J. Phys.: Condens. Matter* **15** 1993

[26] Allen J F 1933 *Philos. Mag.* **16** 1005

[27] Wang J-G, Tian M L, Mallouk Th E and Chan M H W 2004 *Nano Lett.* **4** 1313

[28] Kubiak R and Wołcyrz M 1984 *J. Less-Common Met.* **97** 265